IJNRD.ORG ISSN : 2456-4184
INTERNATIONAL JOURNAL OF NOVEL RESEARCH AND DEVELOPMENT (IJNRD) | IJNRD.ORG
An International Open Access, Peer-reviewed, Refereed Journal

Evaluating The Effects Of Rib Height On The Thermal Dynamics Of Flat Plate Solar Air Heater

1. Junaid Bashar, 2. Dr. Ajay Singh, 3. Prof. Parag Mishra,

1 PG Scholar, Department of Mechanical Engineering, RITS Bhopal, MP, India.
2 Professor & Head, Department of Mechanical Engineering, RITS Bhopal, MP, India.
3 Asst. Professor, Department of Mechanical Engineering, RITS Bhopal, MP, India.

Abstract : In the pursuit of efficient solar collectors for sustainable energy, understanding and optimizing their performance is crucial. This research delves into the impact of rib height variations on the heat transfer properties of a flat plate solar air heater (SAH). The study investigates varying rib heights (2.5 mm, 5 mm, 10 mm, and 15 mm) in a 1500 mm solar collector, using computational fluid dynamics (CFD) simulations with ANSYS software. Results reveal a direct correlation between rib height and free stream velocity, with a maximum of 6.53 m/s for 15 mm high ribs. Velocity near the walls remains static at 0, accompanied by increased boundary layer thickness. Higher rib heights lead to a reduction in the colder region and an increase in average outlet temperature. The 5 mm rib height emerges as the most effective, reaching the highest average outlet temperature at 313.198 K. Turbulent kinetic energy profiles show a positive relationship between rib height and turbulence, with 15 mm high ribs displaying the maximum kinetic energy of 1.03m^2/s^2. Validated through comparison with a base paper, these findings offer comprehensive insights into fluid dynamics and heat transfer in solar collectors, contributing to the design and optimization of efficient solar thermal systems.

IndexTerms **- flat plate solar air heater solar air heater (SAH), computational fluid dynamics (CFD), rib height, boundary layer thickness.**

I. INTRODUCTION

Flat plate solar collectors are devices designed to capture and utilize solar energy for various applications, primarily for heating purposes. These collectors consist of a flat, usually rectangular, absorber plate that is exposed to sunlight, and they are commonly used in solar water heating systems and space heating. Flat plate solar collectors operate on the fundamental principle of harnessing solar energy to generate heat for various applications. These collectors consist of an absorber plate, typically composed of a dark, heat-absorbing material, strategically positioned to receive sunlight. Upon exposure to sunlight, the absorber plate absorbs solar radiation and transforms it into heat. The dark color of the absorber plate enhances its ability to absorb solar energy efficiently.

The absorbed heat is then transferred to a fluid circulating through tubes or channels attached to the absorber plate. Commonly, water or a mixture of water and antifreeze serves as the heat transfer fluid. This heated fluid becomes the carrier of the collected solar energy, circulating through the collector system. A transparent cover, usually made of glass or plastic, shields the absorber plate while allowing sunlight to penetrate. This cover plays a crucial role in minimizing heat loss from the collector, ensuring that the absorbed heat remains within the system. To further mitigate heat loss, the back and sides of the collector are insulated, preserving the temperature of the collected heat.

The applications of the collected solar heat are diverse. In water heating systems, the heated fluid is directed to a storage tank, providing an eco-friendly and energy-efficient source of hot water. For space heating, the collected heat can be circulated through radiant floor or baseboard heating systems. Additionally, flat plate solar collectors find application in various industrial processes requiring heat, such as drying operations. To optimize solar energy absorption, flat plate collectors may be mounted at an angle or equipped with tracking systems, enabling them to follow the sun's path throughout the day. Some systems may incorporate automatic controls to regulate the operation of pumps or fans, ensuring optimal heat transfer and system efficiency. In essence, flat plate solar collectors represent a sustainable and environmentally friendly solution for harnessing solar energy to meet heating needs. By reducing reliance on conventional energy sources and minimizing greenhouse gas emissions, these collectors contribute to the promotion of renewable energy practices. Ongoing technological advancements continue to enhance the efficiency and

versatility of flat plate solar collector systems, further solidifying their role in the transition towards cleaner and more sustainable energy solutions.

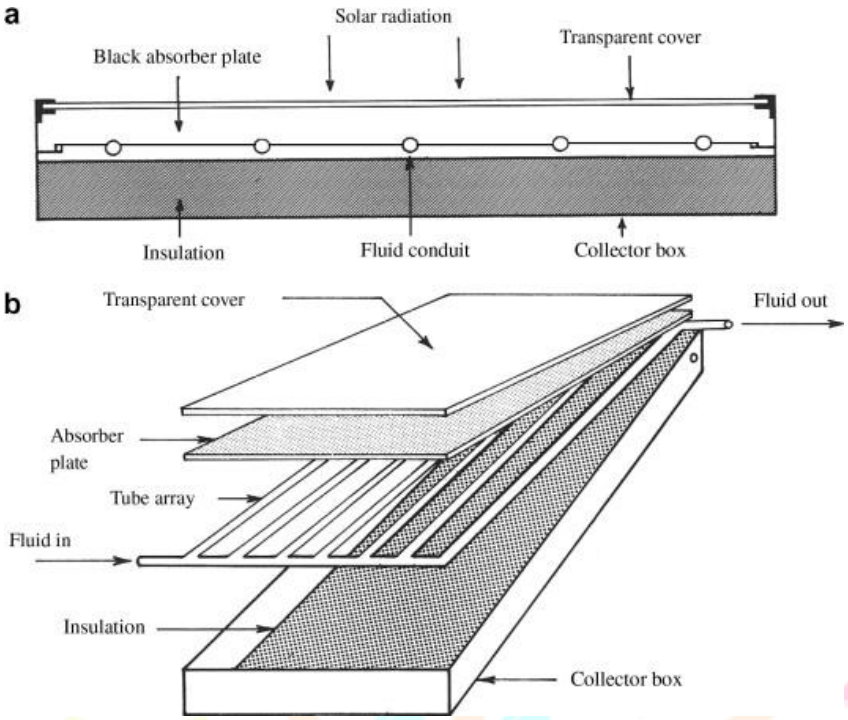

Figure -1 Working of A Flat Plate Solar Collector

This study addresses the pressing need to enhance the efficiency and design of solar air heaters (SAH), crucial components in harnessing renewable energy. Solar collectors are pivotal for converting solar radiation into usable thermal energy, and understanding the intricate factors influencing their performance is essential. The investigation into the effects of rib height on heat transfer properties fills a significant knowledge gap. By delving into variations in rib height and geometry, the study aims to provide valuable insights that can inform the optimization of SAH for improved efficiency. As the demand for sustainable energy solutions rises, this research contributes to advancing the field of solar thermal systems, offering practical knowledge to engineers, researchers, and policymakers working towards a more sustainable and energy-efficient future.

II. LITERATURE SURVEY

In a recent study by Henein and Abdel-Rehim (2022) [1], the thermal performance of an evacuated tube solar collector was assessed using a hybrid nanofluid composed of magnesium oxide and multi-walled carbon nanotubes (MgO/MWCNT). The study considered various weight ratios of MgO/MWCNT nanofluids, ranging from (80:20) to (50:50), and particle concentrations at different flow speeds. Results indicated that increasing the weight ratio of MWCNTs led to enhanced energy and exergy efficiency, with the (50:50) hybrid nanofluid showing a remarkable improvement of 55.83% and 77.14%, respectively. Sethi et al. (2021) [2] addressed thermal needs using evacuated tube solar collectors and explored advancements, including the integration of evacuated-tube collectors with phase-change materials (PCMs). The study highlighted improved thermal energy storage through various PCM inclusion methods, contributing to significant enhancements in outflow temperatures. The review proposed a setup for optimal performance in incorporating PCMs into evacuated tube solar collectors.

Gholipour, Afrand, and Kalbasi (2021) [3] investigated the impact of different absorber tube types coated with a nanofluid of water/silica/ethylene glycol on the thermal efficiency of vacuum tube solar collectors. Results revealed that both spiral and helical-coil tubes increased efficiency, with helical-coil tubes outperforming the others. Economic studies suggested increased costs with spiral and helical-coil tubes, but the addition of nanofluid to the helical coil improved efficiency at a cost. Kumar, Tiwari, and Said (2021) [4] explored various uses of solar thermal energy and focused on the improved performance of evacuated tube solar collectors when incorporating nanofluids and phase-change materials. The study discussed the impact of different geometrical modifications and advanced approaches on the energy, exergy, economic, and environmental aspects of evacuated tube solar collectors.

Olfian, Ajarostaghi, and Ebrahimnataj (2020) [5] delved into the use of nanofluids in solar evacuated tube solar collectors (ETSCs), categorizing them based on various parameters such as types, sizes, and volume fractions of nanofluids. The study provided insights into the most common nanofluids, highlighting their impact on heat transfer in different types of ETSCs. Pawar and Sobhanbandi (2020) [6] investigated the inclusion of phase-change materials (PCMs) in a computational fluid dynamics (CFD) model of a heat pipe evacuated tube collector (HPETC). The study used Tritriacontane paraffin as PCM and demonstrated good agreement between experimental and simulation results, setting benchmarks for HPETCs in thermal energy storage systems. Aramesh and Shabani (2020) [7] conducted a systematic evaluation of phase change materials (PCMs) integrated with evacuated tube solar collectors (ETSCs). The review covered design parameters, integration types, performance, and provided a research plan for these integrated energy systems, addressing pros and cons of different integration methods.

Nidhul et al. (2020) [8] studied the impact of V-ribs on the performance of a triangular solar air heater (SAH) duct using computational fluid dynamics (CFD) and exergy analysis. The inclusion of V-ribs was found to enhance the overall performance of the SAH, and the study compared the ribbed triangular duct SAH with ribbed rectangular duct SAH arrangements. Sharafeldin and Gróf (2019) [9] evaluated the thermal performance of evacuated tube solar collectors using WO3/Water Nanofluid. The study demonstrated that adding WO3 nanoparticles significantly improved collector efficiency, with a 23% increase in maximum heat gain under solar irradiation. The evacuated tube solar collector achieved a thermal-optical efficiency of 72.8%. Mercan and Yurddaş (2019) [10] conducted a numerical analysis of water and water-based nanofluids in evacuated tube solar collectors (ETSCs) using computational fluid dynamics (CFD). The study explored the impacts of different nanofluids on heat transfer under varied conditions, emphasizing the increased heat transmission achieved with CuO–H2O nanofluids.

Naik, Bhowmik, and Muthukumar (2019) [11] presented an experimental research to predict the performance of an evacuated U-tube solar collector. The study demonstrated a basic numerical model for predicting outlet temperature and system efficiency, and empirical correlations were developed for predicting energy efficiency, transition time, and exergy efficiency. Xu et al. (2019) [12] introduced a novel saltwater desalination system using a solar mid-temperature evacuated tube collector. The study highlighted the collector's ability to produce steam with temperatures exceeding 130°C without the need for a solar concentrator, making it a cost-effective solution for mid-temperature steam generation. Jowzi, Veysi, and Sadeghi (2019) [13] enhanced the thermal performance of evacuated tube solar collectors by employing a bypass tube to remove stagnant water from the bottom.

III. DESIGN OF THE FLAT PLATE AIR HEATER DUCT

In this study, a Solar Air Heater (SAH) has been designed, featuring a triangular duct with square cross-section ribs arranged in a "V" configuration. The experimental setup ensures a hydrodynamically developed flow in the initial 500mm entry portion, while minimizing end effects and establishing thermally developed flow through an 800mm test section followed by a 200mm exit section. The Reynolds number (Re), crucial for understanding flow characteristics, is determined by the hydraulic diameter of the duct and spans from 5000 to 20000.

This investigation specifically focuses on an equilateral triangle cross-section with a side length of 76mm. The study delves into the impact of a V-rib, characterized by a rib inclination ranging from 30° to 75°, on heat transmission and friction characteristics. The chosen parameters, including a fixed relative roughness height and a pitch of 22mm, are systematically examined. This research is poised to contribute valuable insights into the nuanced interplay between rib geometry and heat transfer properties within the solar air heater system.

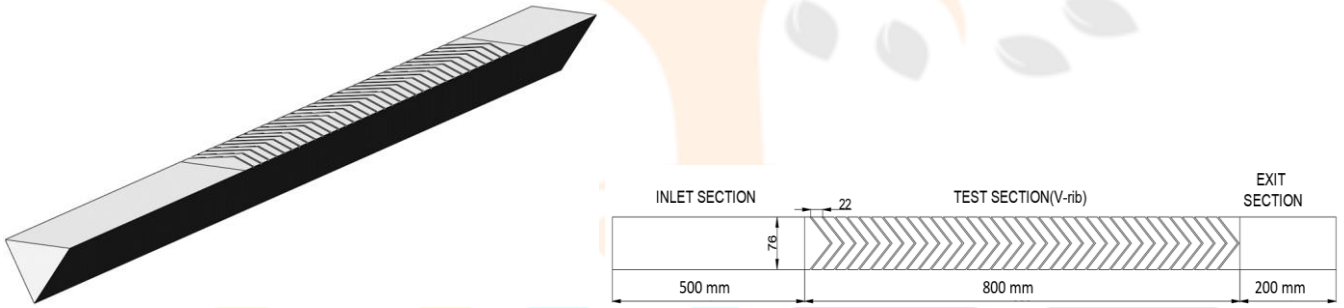

Figure 2 The model of the Flat Plate heat exchanger with rectangular ribs

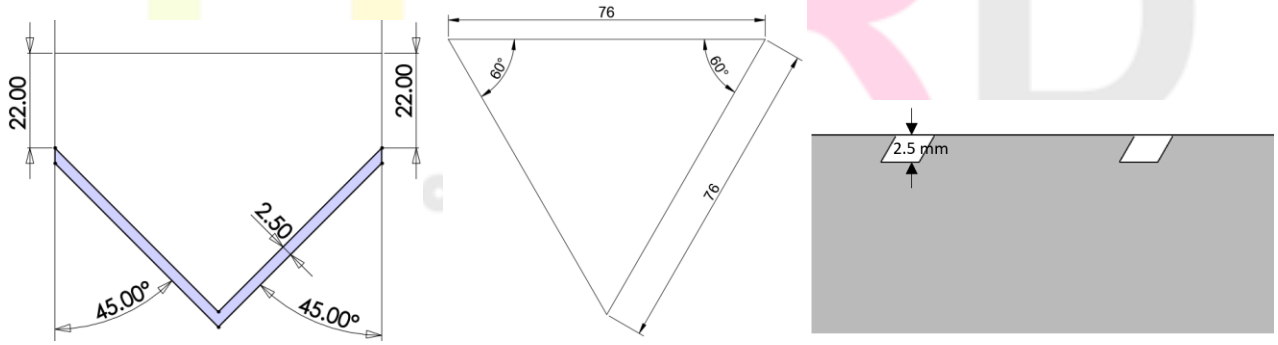

Figure 3 Dimensional details of the rectangular ribs in the test section

IV. CFD ANALYSIS

This study employs a 3-D Computational Fluid Dynamics (CFD) simulation to visually analyze both the flow patterns and heat transfer characteristics along the length of the rib, capturing secondary flows. The governing equations, encompassing momentum, continuity, and energy, are solved using ANSYS with finite volume explicit schemes. Utilizing a second-order upwind strategy and the SIMPLE algorithm for discretization, the simulation adopts the RNG k- turbulence model with "enhanced wall treatment" (EWT), a choice supported by previous CFD research in ribbed Solar Air Heaters (SAH).

The numerical investigation ensures the preservation of mass, momentum, and energy in the final solution. Throughout the simulation, the plate's mean pressure and temperature variations are measured after each cycle. This comprehensive approach provides a robust foundation for understanding the intricate dynamics of ribbed SAH, contributing valuable insights to the field of thermal-fluid analysis.

a. Mesh Generation

To accurately represent the physical shape of an object within its continuous geometric space, the intricate details are meticulously analyzed by decomposing it into thousands or more distinct shapes. In 3D CAD models, achieving a higher level of precision and simulation accuracy is facilitated by utilizing denser meshes. Meshing, a fundamental process in this context, involves breaking down a complex shape into smaller, more manageable components. Mesh generation can produce either two or three-dimensional meshes.

Given that meshing consumes a substantial amount of time in obtaining simulation results, the adoption of automated approaches becomes crucial for enhancing efficiency and result accuracy. In the specific case at hand, the total node count reaches 45,837, while the number of elements amounts to 194,342. This meticulous meshing process ensures a detailed and reliable representation of the object's geometry, laying the groundwork for more effective and precise simulations.

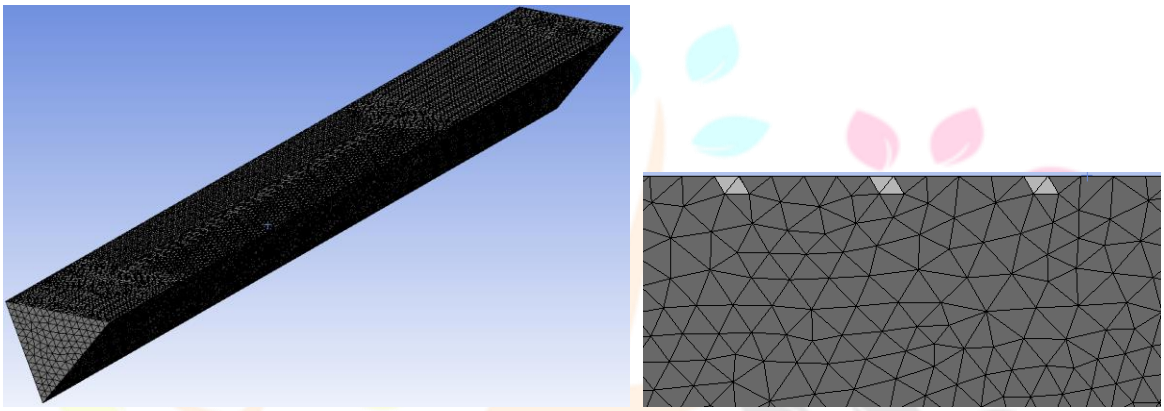

Figure 4 Meshing of the Heat Exchanger

b. Boundary Conditions

- Energy ON
- RNG K-e turbulence model (enhance wall treatment)
- Hydraulic Diameter (D_h) = 0.044 [m]
- Fix heat flux is applied at absorber plate
- Inlet Velocity = 2.74 m/s (Re = 7500)
- Inlet air temperature is selected as 303.15 [K]
- Pressure outlet temperature is selected

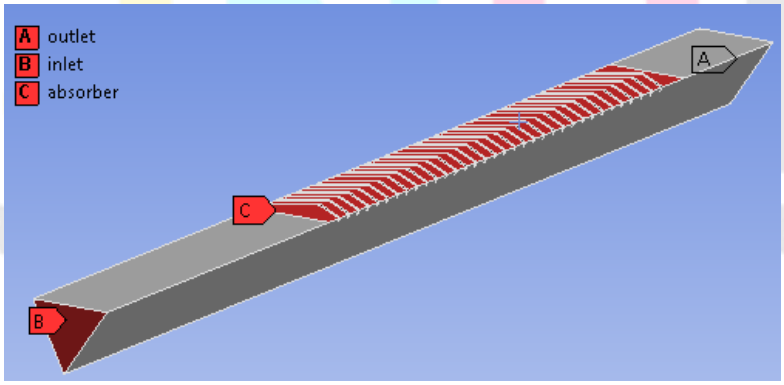

Figure 5 Boundary Conditions applied on the heat exchanger

V. VALIDATION CASE

To validate our findings, a meticulous comparison was conducted, focusing on the temperature analysis results presented in the foundational work by (Nidhul et al., 2020)[8]. The temperatures derived from both our study and the referenced work consistently fell within the range of 303 to 327 K. This alignment affirms the accuracy and precision of our simulation methodology, validating not only the chosen parameters but also ensuring the reliability of our results. The congruence in temperature ranges further establishes the robustness of our approach, providing confidence in the overall accuracy of the outcomes.

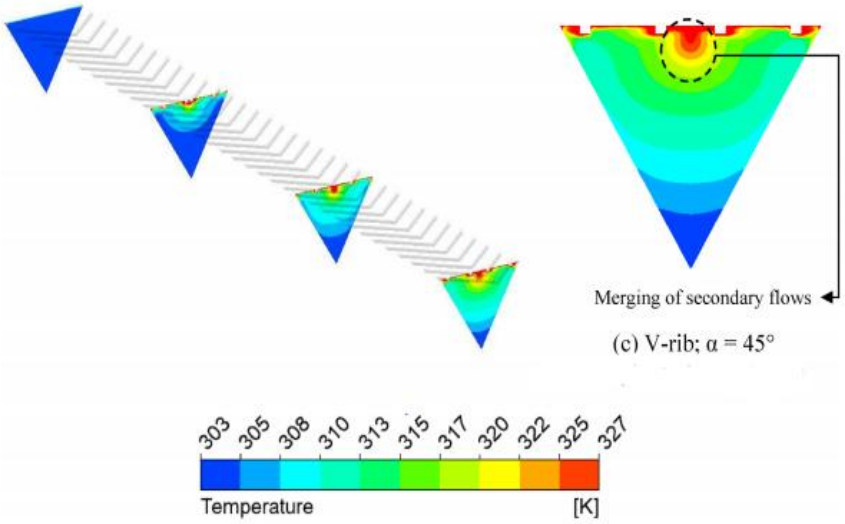

Figure 6 Results of the Base Paper

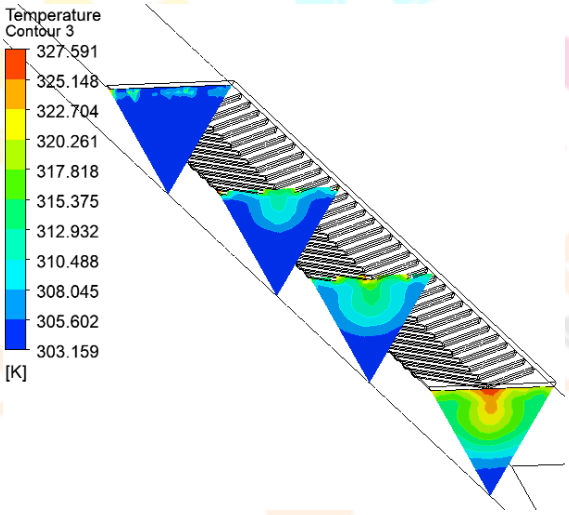

Figure -7 Results for the model used in this work

VI. RESULTS FOR RECTANGULAR RIBS WITH DIFFERENT HEIGHTS

a. Temperature Contours

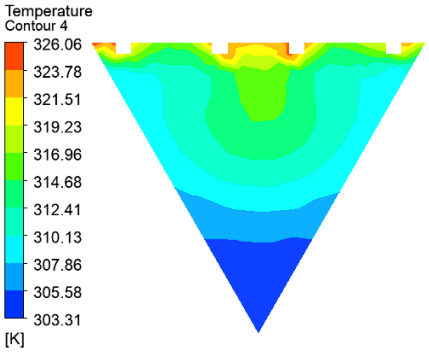

(a) 2.5 mm Rib Height

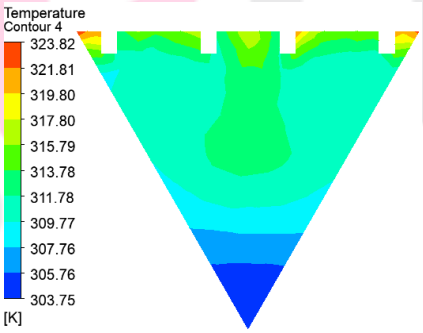

(b) 5 mm Rib Height

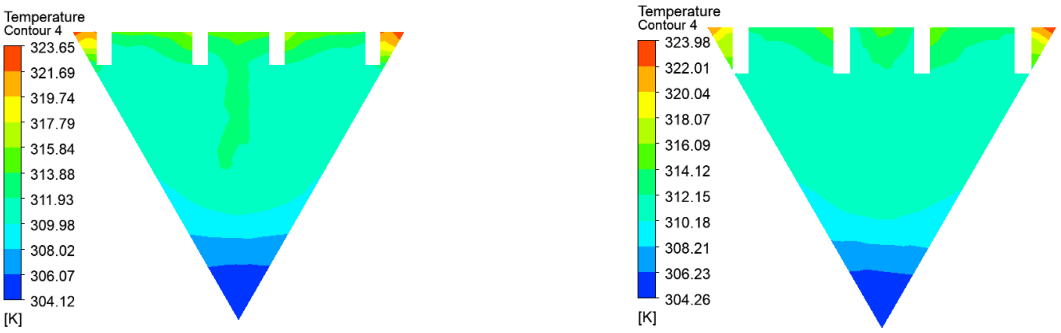

(c) 10 mm Rib Height **(d) 15 mm Rib Height**

Figure -8 (a) 2.5 mm Rib Height, (b) 5 mm Rib Height, (c) 10 mm Rib Height, (d) 15 mm Rib Height

Table -1 Average Outlet temperature in different cases of ribs having different heights

Type	Average Outlet Temperature[K]
2.5 mm Rib Height	310.68
5 mm Rib Height	313.21
10 mm Rib Height	312.97
15 mm Rib Height	313.06

Analysis of temperature contours along the triangular cross-section, depicted in Figure 4-3, reveals noteworthy patterns. The colder region diminishes with escalating rib height. Notably, beyond a rib height of 2.5 mm, the temperature near rib walls decreases. However, an interesting observation is that, despite this localized cooling effect, the average fluid temperature at the outlet registers an overall increase with higher rib heights. For a 5 mm high rib, the maximum average outlet temperature is recorded at 313.198 K, underscoring the influence of rib height on the thermal characteristics of the system.

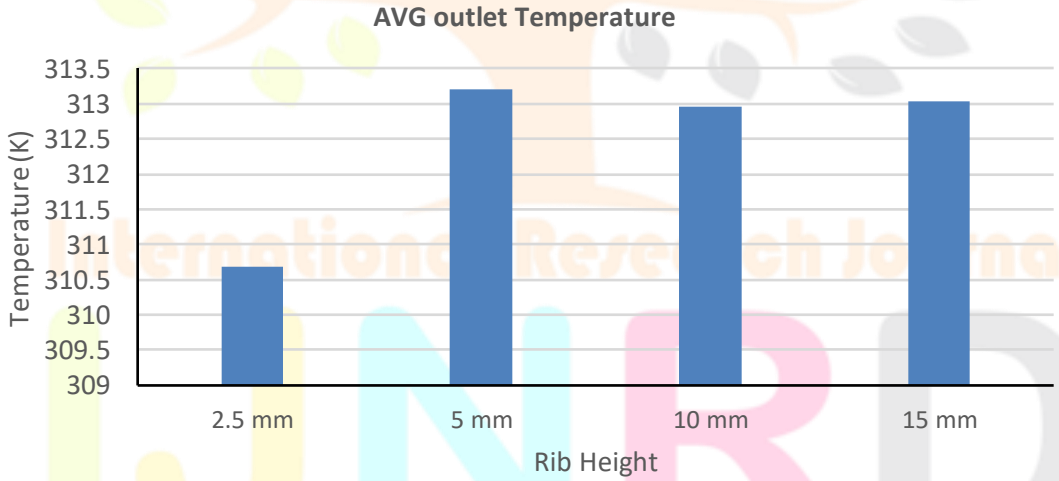

Figure -9 Comparison of the average outlet temperature for different heights

b. Velocity Contours

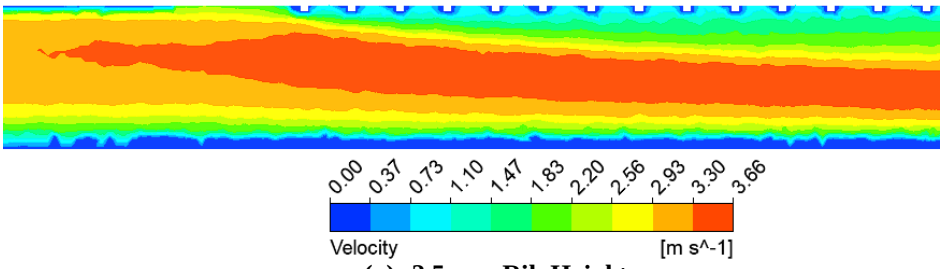

(a) 2.5 mm Rib Height

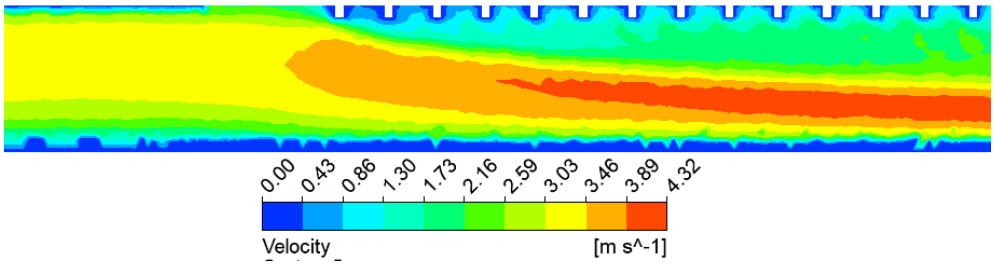

(b) 5 mm Rib Height

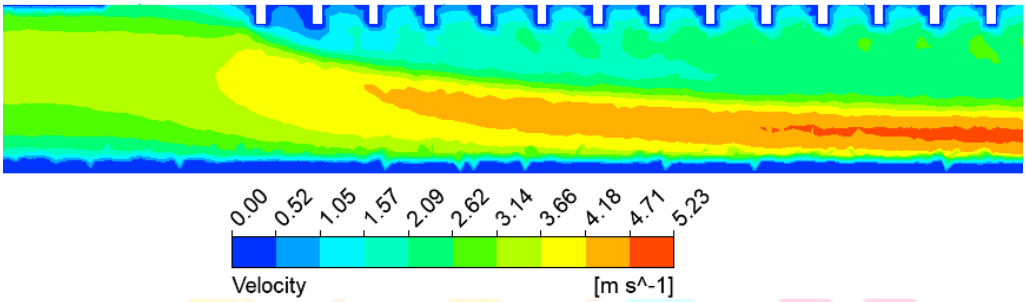

(c) 10 mm Rib Height

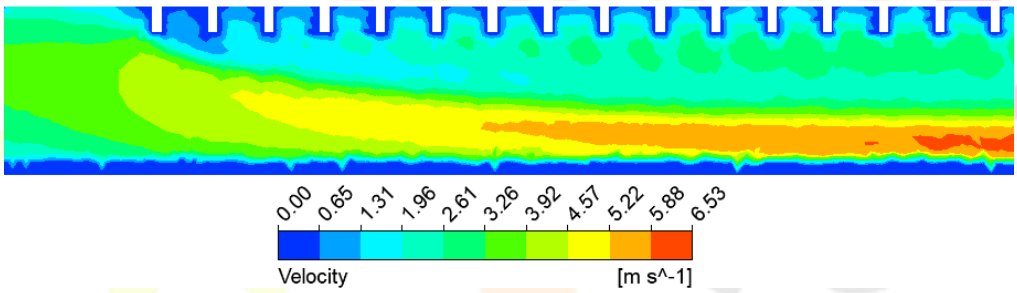

(d) 15 mm Rib Height

Figure -10 (a) 2.5 mm Rib Height, (b) 5 mm Rib Height, (c) 10 mm Rib Height, (d) 15 mm Rib Height

Examining the velocity contours in Figure 4-5 provides insights into the impact of rib height on flow dynamics. Notably, an increase in rib height correlates with a rise in the maximum free stream velocity – ascending from 3.66 m/s for a 2.5 mm high rib to 6.53 m/s for a 10 mm high rib. This elevation in rib height also leads to a substantial augmentation in the thickness of boundary layers adjacent to rib walls, resulting in a notably slender flow width in the free stream. The boundary layer thickness is at its minimum with a 2.5 mm high rib and peaks with a 15 mm high rib, emphasizing the nuanced interplay between rib height and boundary layer characteristics. However, an intriguing revelation surfaced regarding the velocity near the walls, which consistently maintained a value of 0. Simultaneously, an augmentation in the thickness of the boundary layer was observed with an increase in rib height. This insight is crucial for understanding the complex fluid dynamics within the solar collector.

Table -2 Maximum Velocity in different cases of ribs having different heights

Type	Maximum Velocity (ms^{-1})
2.5 mm Rib Height	3.66
5 mm Rib Height	4.32
10 mm Rib Height	5.23
15 mm Rib Height	6.53

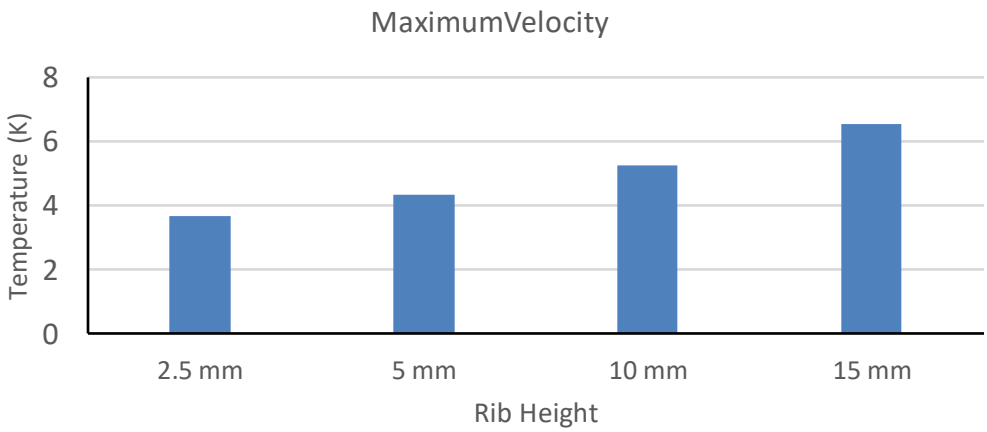

Figure -11 Comparison of the maximum velocities for different heights

c. Turbulence Kinetic Energy Contours

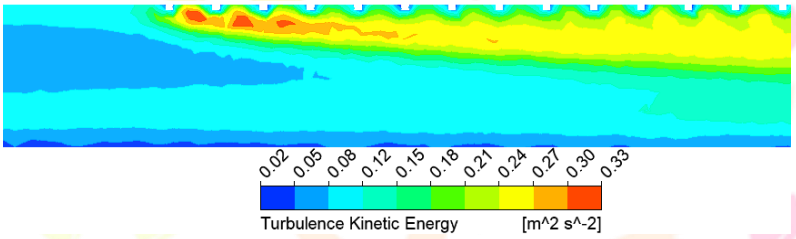

(a) 2.5 mm Rib Height

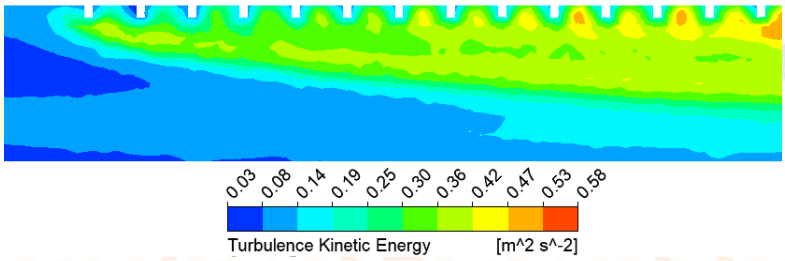

(b) 5 mm Rib Height

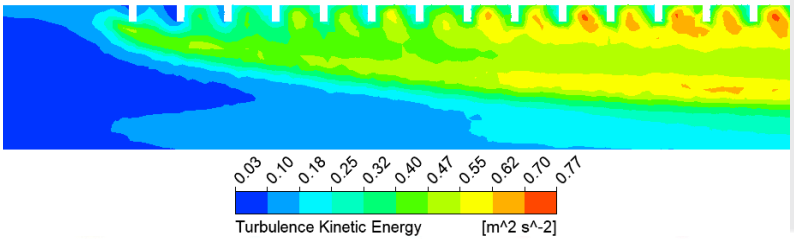

(c) 10 mm Rib Height

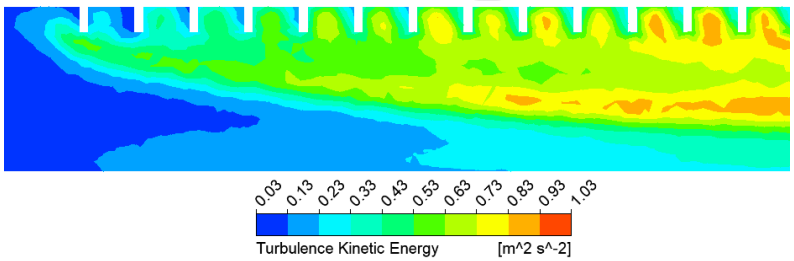

(d) 15 mm Rib Height

Figure-12 (a) 2.5 mm Rib Height, (b) 5 mm Rib Height, (c) 10 mm Rib Height, (d) 15 mm Rib Height

Examining turbulence kinetic energy values, illustrated in Figure 4-7, reveals a consistent escalation with rib height. This phenomenon is attributed to the heightened obstacle effect posed by taller ribs, intensifying flow turbulence. The pinnacle of

turbulence kinetic energy is observed with 15 mm high ribs, registering at 1.03 m²/s², while the minimum is recorded for 2.5 mm high ribs at 0.33 m²/s². Notably, turbulence kinetic energy undergoes a sharp ascent in the mid-length of the solar collector test section, gradually subsiding towards the outlet. This observed trend reaffirms that taller ribs contribute to increased turbulence throughout the flow, underscoring the direct correlation between rib height and turbulence levels. A discernible pattern emerged as turbulent kinetic energy exhibited an ascent towards the midsection before gradually diminishing towards the outlet.

Table -3 Maximum Kinetic Energy in different cases of ribs having different heights

Type	Maximum Kinetic Energy(m^2/s^2)
2.5 mm Rib Height	0.33
5 mm Rib Height	0.58
10 mm Rib Height	0.77
15 mm Rib Height	1.03

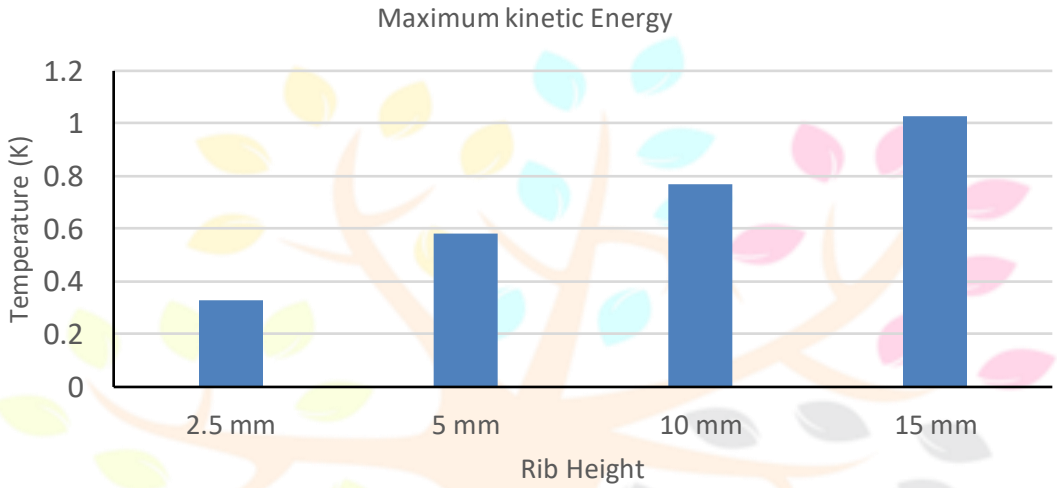

Figure -13 Comparison of the maximum velocities for different heights

VII. CONCLUSION

In the study, a solar collector with a total length of 1500 mm was carefully divided into distinct sections, comprising a 500 mm inlet, an 800 mm midsection designated as the test section, and a 200 mm outlet. The test section was equipped with ribs featuring a uniform thickness of 2.5 mm and spaced at intervals of 22 mm. To comprehensively evaluate the thermal performance, various rib heights were considered, ranging from 2.5 mm to 15 mm.

- An insightful observation emerged concerning the impact of rib height on the free stream's maximum velocity, all under identical inlet conditions. The results demonstrated a noticeable increase in the maximum free stream velocity as the rib height ascended. Specifically, the velocity surged from 3.66 m/s for the 2.5 mm high ribs to an elevated 6.53 m/s for the 15 mm high ribs.

- The correlation between rib height and kinetic energy became apparent, with higher ribs corresponding to increased kinetic energy. The pinnacle was reached with 15 mm high ribs, registering a maximum kinetic energy of1.03 m²/s². This phenomenon was attributed to the heightened turbulence induced by the larger dimensions of the ribs.

- Among the various rib heights investigated, the average temperature at the outlet reached its zenith with 5 mm high ribs, registering an impressive 313.21 K. This observation led to the identification of 5 mm rib height as the most effective in terms of thermal performance. Consequently, this specific rib height was earmarked for further analysis, encompassing different rib shapes, namely rectangular, triangular, and circular.

In summary, the meticulous examination of the solar collector's performance, considering rib height variations and subsequent analyses with different rib shapes, provided a comprehensive understanding of the thermal dynamics at play. The insights gained not only shed light on the optimal conditions for maximizing free stream velocity, turbulent kinetic energy, and average temperature but also set the stage for future advancements in solar collector design and efficiency.

REFERENCES

[1] S. M. Henein and A. A. Abdel-Rehim, "The performance response of a heat pipe evacuated tube solar collector using MgO/MWCNT hybrid nanofluid as a working fluid," *Case Stud. Therm. Eng.*, vol. 33, no. March, p. 101957, 2022, doi: 10.1016/j.csite.2022.101957.

[2] M. Sethi *et al.*, "Recent developments in design of evacuated tube solar collectors integrated with thermal energy storage: A review," *Mater. Today Proc.*, 2021, doi: https://doi.org/10.1016/j.matpr.2021.11.324.

[3] S. Gholipour, M. Afrand, and R. Kalbasi, "Introducing two scenarios to enhance the vacuum U-tube solar collector efficiency by considering economic criterion," *J. Taiwan Inst. Chem. Eng.*, vol. 124, pp. 228–237, 2021, doi: 10.1016/j.jtice.2021.04.015.

[4] A. Kumar, A. K. Tiwari, and Z. Said, "A comprehensive review analysis on advances of evacuated tube solar collector using nanofluids and PCM," *Sustain. Energy Technol. Assessments*, vol. 47, no. July, p. 101417, 2021, doi: 10.1016/j.seta.2021.101417.

[5] H. Olfian, S. S. M. Ajarostaghi, and M. Ebrahimnataj, "Development on evacuated tube solar collectors: A review of the last decade results of using nanofluids," *Sol. Energy*, vol. 211, no. July, pp. 265–282, 2020, doi: 10.1016/j.solener.2020.09.056.

[6] V. R. Pawar and S. Sobhansarbandi, "CFD modeling of a thermal energy storage based heat pipe evacuated tube solar collector," *J. Energy Storage*, vol. 30, no. January, p. 101528, 2020, doi: 10.1016/j.est.2020.101528.

[7] M. Aramesh and B. Shabani, "On the integration of phase change materials with evacuated tube solar thermal collectors," *Renew. Sustain. Energy Rev.*, vol. 132, no. February, p. 110135, 2020, doi: 10.1016/j.rser.2020.110135.

[8] K. Nidhul, S. Kumar, A. K. Yadav, and S. Anish, "Enhanced thermo-hydraulic performance in a V-ribbed triangular duct solar air heater: CFD and exergy analysis," *Energy*, vol. 200, p. 117448, 2020, doi: 10.1016/j.energy.2020.117448.

[9] M. A. Sharafeldin and G. Grófˊ, "Efficiency of evacuated tube solar collector using WO3/Water nanofluid," *Renew. Energy*, vol. 134, pp. 453–460, 2019, doi: 10.1016/j.renene.2018.11.010.

[10] M. Mercan and A. Yurddaş, "Numerical analysis of evacuated tube solar collectors using nanofluids," *Sol. Energy*, vol. 191, no. July, pp. 167–179, 2019, doi: 10.1016/j.solener.2019.08.074.

[11] B. K. Naik, M. Bhowmik, and P. Muthukumar, "Experimental investigation and numerical modelling on the performance assessments of evacuated U – Tube solar collector systems," *Renew. Energy*, vol. 134, pp. 1344–1361, 2019, doi: 10.1016/j.renene.2018.09.066.

[12] L. C. Xu, Z. H. Liu, S. F. Li, Z. X. Shao, and N. Xia, "Performance of solar mid-temperature evacuated tube collector for steam generation," *Sol. Energy*, vol. 183, no. January, pp. 162–172, 2019, doi: 10.1016/j.solener.2019.03.022.

[13] M. Jowzi, F. Veysi, and G. Sadeghi, "Experimental and numerical investigations on the thermal performance of a modified evacuated tube solar collector: Effect of the bypass tube," *Sol. Energy*, vol. 183, no. September 2018, pp. 725–737, 2019, doi: 10.1016/j.solener.2019.03.063.

[14] A. Kotb, M. B. Elsheniti, and O. A. Elsamni, "Optimum number and arrangement of evacuated-tube solar collectors under various operating conditions," *Energy Convers. Manag.*, vol. 199, no. September, p. 112032, 2019, doi: 10.1016/j.enconman.2019.112032.

[15] R. Elbahjaoui, H. El Qarnia, and A. Naimi, "Thermal performance analysis of combined solar collector with triple concentric-tube latent heat storage systems," *Energy Build.*, vol. 168, pp. 438–456, 2018, doi: 10.1016/j.enbuild.2018.02.055.

[16] J. J. Ramírez-Minguela *et al.*, "Comparison of the thermo-hydraulic performance and the entropy generation rate for two types of low temperature solar collectors using CFD," *Sol. Energy*, vol. 166, no. March, pp. 123–137, 2018, doi: 10.1016/j.solener.2018.03.050.

[17] G. Martínez-Rodríguez, A. L. Fuentes-Silva, and M. Picón-Núñez, "Solar thermal networks operating with evacuated-tube collectors," *Energy*, vol. 146, pp. 26–33, 2018, doi: 10.1016/j.energy.2017.04.165.

[18] I. M. Mahbubul, M. M. A. Khan, N. I. Ibrahim, H. M. Ali, F. A. Al-Sulaiman, and R. Saidur, "Carbon nanotube nanofluid in enhancing the efficiency of evacuated tube solar collector," *Renew. Energy*, vol. 121, pp. 36–44, 2018, doi: 10.1016/j.renene.2018.01.006.

[19] S. Sobhansarbandi, P. M. Martinez, A. Papadimitratos, A. Zakhidov, and F. Hassanipour, "Evacuated tube solar collector with multifunctional absorber layers," *Sol. Energy*, vol. 146, pp. 342–350, 2017, doi: 10.1016/j.solener.2017.02.038.

[20] M. A. Essa and N. H. Mostafa, "Theoretical and experimental study for temperature distribution and flow profile in all water evacuated tube solar collector considering solar radiation boundary condition," *Sol. Energy*, vol. 142, pp. 267–277, 2017, doi: 10.1016/j.solener.2016.12.035.